The Astrophysical Journal Supplement Series, 169:225–238, 2007 April


# MULTIAPERTURE *UBVRIzJHK* PHOTOMETRY OF GALAXIES IN THE COMA CLUSTER

Peter R. Eisenhardt,[1,2] Roberto De Propris,[3] Anthony H. Gonzalez,[4] S. A. Stanford,[5,6]
Michael Wang,[7] and Mark Dickinson[8]

*Received 2006 October 18; accepted 2006 November 28*

## ABSTRACT

We present a set of *UBVRIzJHK*$_s$ photometry for 745 $J + H$–band–selected objects in a $22.5' \times 29.2'$ region centered on the core of the Coma Cluster. This includes 516 galaxies and is at least 80% complete to $H = 16$, with a spectroscopically complete sample of 111 cluster members (nearly all with morphological classification) for $H < 14.5$. For each object we present total Kron (1980) magnitudes and aperture photometry. As an example, we use these data to derive color-magnitude relations for Coma early-type galaxies, measure the intrinsic scatter of these relations and its dependence on galaxy mass, and address the issue of color gradients. We find that the color gradients are mild and that the intrinsic scatter about the color-magnitude relation is small ($\sim$0.05 mag in $U - V$ and less than $\sim$0.03 in $B - R$, $V - I$, or $J - K$). There is no evidence that the intrinsic scatter varies with galaxy luminosity, suggesting that the cluster red sequence is established at early epochs over a range of $\sim$100 in stellar mass.

*Subject headings:* galaxies: clusters: individual (Coma) — galaxies: evolution — galaxies: formation — galaxies: photometry

*Online material:* machine-readable tables

## 1. INTRODUCTION

Clusters of galaxies may provide the database needed for a coherent theory of galaxy evolution, in the same way that clusters of stars meet this need for stellar evolution. Environmental effects such as tidal interactions and mergers, ram pressure stripping, and confinement of gas by the intracluster medium (to name a few) make galaxy clusters more complex than their stellar counterparts. However, the great luminosities of galaxy clusters (and galaxies) compensate for such complications by making it possible to directly observe their evolution to large look-back times (for instance, Stanford et al. 1995, 1998; De Propris et al. 1999; Holden et al. 2004; Strazzullo et al. 2006), a luxury impractical at present for stars.

This hope has already been somewhat realized in a surprisingly straightforward fashion, using the familiar color-magnitude diagram. A well-defined "main sequence" of luminous early-type galaxies is evident in nearby clusters and appears to have the same slope and scatter in all systems (Sandage & Visvanathan 1978; Bower et al. 1992 [hereafter BLE92]; Terlevich et al. 2001; Lopez-Cruz et al. 2004; McIntosh et al. 2005) and can be observed, essentially unchanged, at least to the highest redshifts studied (Stanford et al. 1995, 1998; Kajisawa et al. 2000; van Dokkum et al. 2000, 2001; Blakeslee et al. 2003; Holden et al. 2004, 2006; Lidman et al. 2004; Wake et al. 2005; Ellis et al. 2006; Mei et al. 2006a, 2006b).

The color-magnitude relation (CMR) appears to be mainly due to a relation between mass and metal abundance (Trager et al. 2000; Terlevich et al. 2001). Its existence and low scatter may provide a stringent test of theories of galaxy formation (Kaviraj et al. 2005; Renzini 2006). The observations imply a remarkably synchronized star formation history for early-type galaxies across a wide range of environments, which can be straightforwardly modeled by an initial burst of formation at high redshift followed by passive evolution of the stellar population, similar to the early monolithic collapse scenario of Eggen et al. (1962).

Measuring such changes with look-back time requires reference to color-magnitude data at the same rest wavelengths at redshift zero. The standard of reference used in Stanford et al. (1998), as well as many other similar studies, was the Coma Cluster. Rich in early-type galaxies and with a look-back time of only about 300 Myr, multiband (*UBVRIzJHK*) observations of the Coma Cluster were compared to observations of clusters with large look-back times using *interpolated k*-corrections. Selecting galaxies by their near-infrared luminosity is desirable because this is representative of stellar mass (Gavazzi et al. 1996; Bell & de Jong 2001) and is relatively insensitive to dust and minor starbursts. The typical size of the fields observed by Stanford et al. (1995, 1998) and of the *Hubble Space Telescope* (*HST*) field of view at the redshifts of the clusters is about 1 Mpc. For the Coma Cluster, 1 Mpc corresponds to $\sim 30'$ ($H_0 = 67$). Hence, obtaining and reducing the reference data, particularly in the near-infrared, was a challenging project. Because we expect that other workers will find an infrared-selected catalog of *UBVRIzJHK* Coma Cluster photometry useful, we are publishing these data as a separate paper, with minimal analysis. Several studies in the literature (e.g., Shioya et al. 2002; Ellis et al. 2006) have used this database prior to publication, and we believe that this data set will be useful for the general community. We have previously presented a study of the infrared luminosity function of Coma galaxies (De Propris et al. 1998).

The structure of this paper is as follows: § 2 presents our observations and data reduction; § 3 presents the photometric catalog; and § 4 provides an analysis of color-magnitude relations and their intrinsic scatter, and a brief discussion of the implications for galaxy formation models. All photometry is on the Vega system. For consistency with our previous work (Stanford et al. 1995, 1998), we adopt a cosmology with $H_0 = 67\ \mathrm{km\ s^{-1}\ Mpc^{-1}}$,

[1] Jet Propulsion Laboratory, California Institute of Technology, Pasadena, CA 91109.
[2] California Institute of Technology, Pasadena, CA 91125.
[3] Cerro Tololo Inter-American Observatory, La Serena, Chile.
[4] Department of Astronomy, University of Florida, Gainesville, FL 32611.
[5] Physics Department, University of California, Davis, CA 95616.
[6] Institute of Geophysics and Planetary Physics, Lawrence Livermore National Laboratories, Livermore, CA 94550.
[7] Kingbright Electronics, Chung Ho, Taipei Hsien, Taiwan.
[8] National Optical Astronomy Observatory, Tucson, AZ 85719.

FIG. 1.—*UVK* color image of the Coma field used in this study, showing *U* (*blue*), *V* (*green*), and *K* (*red*). The image is centered on approximately $12^h59^m52.8^s$, $+27^\circ55'00''$ (J2000.0) and subtends $29.2'$(R.A.)$\times 22.5'$(decl.). North is up, and east is to the left. The calibrated fits image mosaics are available through the NOAO Science Archive.

$q_0 = 0.1$, and $\Lambda_0 = 0$. Adopting a redshift of 0.023, this gives a luminosity distance of 104 Mpc and an angular scale of $0.482''$ kpc$^{-1}$. For the commonly used $H_0 = 70$ km s$^{-1}$ Mpc$^{-1}$, $\Omega_M = 0.3$, $\Lambda_0 = 0.7$ cosmology, the corresponding values are 100.2 and 0.464, respectively.

## 2. OBSERVATIONS AND DATA REDUCTION

### 2.1. *Infrared Imaging*

Infrared imaging at *J*, *H*, and $K_s$ was obtained using the IRIM camera, with a $256\times256$ NICMOS3 HgCdTe array at the Kitt Peak National Observatory (KPNO) 2.1 m telescope on the night of 1993 April 7. The pixels subtended $\approx1.1''$, with the scale being slightly different in each band. A $12\times9$ frame mosaic with $133''$ steps (i.e., $\approx$53% overlap) between frames in both axes was obtained in each band, spanning $29.2'$(R.A.)$\times22.5'$(decl.) centered on approximately $12^h59^m52.8^s$, $+27^\circ55'00''$ (J2000.0). The specific area was chosen to include the highest density region in the tabulation of Dressler (1980), including Dressler's Nos. 82, 91, and 168 (corresponding to Nos. 6, 26, and 16, respectively, in our catalog) near the edges of the region. Two frames were omitted from the mosaic: the *H* frame centered near $12^h59^m57.4^s$, $+28^\circ01'39''$ had an anomalous sky level in one quadrant, and the *K* frame centered near $12^h59^m18.1^s$, $+27^\circ57'13''$ was lost in the data transfer process.

The exposure time per frame was 15 s for *J* and $K_s$ and 10 s for *H*. The mosaic corners were only sampled once, other positions along the edge were sampled twice, and positions more than $133''$ from the edge of the mosaic were sampled 4 times, resulting in a nominal total exposure time over most of the field of 60, 40, and 60 s in *J*, *H*, and $K_s$, respectively. Figure 1 shows a *UVK* mosaic of the entire survey region produced from our data.

The images, which were taken using double correlated sampling, were linearized using an empirical correction developed for each pixel, and then flat-fielded. A $7\times7$ grid of observations of M67 was used to determine the type of flat-field exposure that minimized the photometric dispersion in measurements of the same stars at many locations across the array. For *J* and *H* median sky flats worked best, while for $K_s$ an average of dome flats with ambient illumination (i.e., lights off) minimized the dispersion, which was $\approx$2% for all three bands. Next the DIMSUM[9] package within IRAF was used to carry out sky subtraction and masking of bad pixels and cosmic-ray hits. For each frame, DIMSUM calculates a median sky frame from preceding and following frames, masking pixels associated with detectable objects. In the

[9] Deep Infrared Mosaicing Software, developed by P. Eisenhardt, M. Dickinson, S. A. Stanford, and J. Ward, available at ftp://iraf.noao.edu/iraf/contrib/dimsum.tar.Z.

TABLE 1
MAIN CATALOG OF COMA OBJECTS

| ID (1) | R.A. (J2000.0) (2) | Decl. (J2000.0) (3) | $H$ (4) | Type (5) | Ref. (6) | $cz$ (km s$^{-1}$) (7) | Ref. (8) | GMP83 (9) | NGC/IC/RB/D (10) | Notes (11) |
|---|---|---|---|---|---|---|---|---|---|---|
| 1 | 13 00 08.06 | 27 58 37.4 | 9.14 | Db | D80[a] | 6495. | M02[b] | 2921. | NGC4889, D148 | |
| 2 | 13 00 48.41 | 27 48 03.6 | 9.51 | Star | | 0. | | 0. | | |
| 3 | 12 59 35.62 | 27 57 34.1 | 9.60 | cD | D80 | 7224. | S00 | 3329. | NGC4874, D129 | |
| 4 | 12 58 56.78 | 27 51 31.4 | 10.23 | Star | | 0. | | 0. | | |
| 5 | 12 59 28.85 | 27 56 14.4 | 10.23 | Star | | 0. | | 0. | | |
| 6 | 13 00 55.99 | 27 47 26.6 | 10.25 | Sb | D80 | 7985. | H97 | 2374. | NGC4911, D82 | |
| 7 | 12 59 20.52 | 27 51 42.1 | 10.54 | Star | | 0. | | 0. | | |
| 8 | 13 00 54.33 | 28 00 28.1 | 10.55 | E | D80 | 8793. | S00 | 2417. | IC4051, D143 | |
| 9 | 13 00 41.60 | 27 50 39.6 | 10.62 | Star | | 0. | | 0. | | |
| 10 | 12 59 19.80 | 28 05 03.9 | 10.62 | E | D80 | 4700. | S04 | 3561. | NGC4865, D179 | |

NOTE.—Units of right ascension are hours, minutes, and seconds, and units of declination are degrees, arcminutes, and arcseconds. Table 1 is published in its entirety in the electronic edition of the *Astrophysical Journal Supplement*. A portion is shown here for guidance regarding its form and content.

[a] Morphology references.—(D80) Dressler 1980; (RB) Rood & Baum 1967; (C93) Caldwell et al. (1993; (GG) Graham & Guzman 2003.

[b] Redshift references.—(A00) Adami et al. 2000; (B95) Biviano et al. 1995; (C93) Caldwell et al. 1993; (C96) Casoli et al. 1996; (CD) Colless & Dunn 1996; (C01) Castander et al. 2001; (D88) Dressler & Shectman 1988; (E02) Edwards et al. 2002; (H97) Haynes et al. 1997; (M99) Müller et al. 1999; (MG) Matkovic & Guzman 2005; (M01) Mobasher et al. (2001; (M02) Moore et al. 2002; (S00) Smith et al. (2000; (S04) Smith et al. 2004.

$J$ band a median of 10 surrounding frames while rejecting the two highest and two lowest values at each pixel was found to produce the most uniform appearance across the final mosaicked image. For $H$ a median of 14 frames with rejection of the three highest and three lowest pixels worked best. For $K_s$ an eight-frame median and rejecting two high and two low pixels was used for the top and bottom thirds of the mosaic. Because of the large extent of the two dominant central galaxies (NGC 4874 and NGC 4889), in the center three rows of the mosaic DIMSUM tended to oversubtract the sky, and using a median that rejected a larger number of frames substantially alleviated this problem. Nevertheless, the extended emission near these two galaxies has probably been suppressed to some extent.

Registration of each sky-subtracted frame to the nearest half-pixel was accomplished using offsets measured from objects that overlapped with those in frames to the south or east. The resulting three IR mosaics were registered to one another and rebinned to a common pixel size of 0.6845″ using astrometry for 78 *HST* Guide Star Catalog objects within the field. In the process the pixel scale for IRIM on the KPNO 2.1 m was determined to be $1.0996'' \pm 0.0005''$, $1.0964'' \pm 0.0005''$, and $1.0922'' \pm 0.0005''$ pixel$^{-1}$ in $J$, $H$, and $K_s$, respectively.

Multiple observations of five United Kingdom Infrared Telescope (UKIRT) standards transformed to the California Institute of Technology system (Elias et al. 1982) established that the IR data were photometric and that the extinction coefficients were 0.17, 0.07, and 0.09 mag per air mass in $J$, $H$, and $K_s$, respectively. The Coma mosaic data were all obtained at air mass $<1.15$. Comparison with the infrared photometry of Persson et al. (1979, hereafter PFA79; see below) showed no convincing evidence for a color term but did reveal the need for a correction of 2%–4% for light lost in the small (5.5″ diameter) apertures used in measuring the relatively faint UKIRT standard stars. This aperture correction was determined empirically from an average of over 50 brighter stars in the standard star images. The zero points are judged to be accurate to $\pm 0.03$ mag.

### 2.2. *Optical Data*

Optical data were obtained during service observations by G. Jacoby at the KPNO 0.9 m telescope on 1994 March 15 and 16 using a $2048^2$ CCD with 0.680″ pixels. Exposures in $B$, $V$, $R$, and $I$ were obtained in two positions to cover the infrared mosaic, whereas three positions were used for $U$ and $z$. The total exposure times were 5400 s in $U$, 1200 s in $B$, 500 s in $V$ and $R$, 300 s in

TABLE 2
TOTAL MAGNITUDES FOR COMA OBJECTS

| ID (Table 1) | $U$ | $B$ | $V$ | $R$ | $I$ | $z$ | $J$ | $H$ | $K$ |
|---|---|---|---|---|---|---|---|---|---|
| 1[a] | 13.83 | 13.27 | 12.24 | 11.65 | 10.91 | 10.59 | 9.86 | 9.14 | 8.88 |
| 2 | 13.88 | 13.64 | 12.79 | 12.65 | 11.56 | 11.54 | 10.12 | 9.51 | 9.76 |
| 3[a] | 14.24 | 13.74 | 12.71 | 12.12 | 11.39 | 11.03 | 10.37 | 9.60 | 9.41 |
| 4 | 13.51 | 13.47 | 12.88 | 12.75 | 11.78 | 11.70 | 10.65 | 10.23 | 10.24 |
| 5 | 14.68 | 14.09 | 13.20 | 12.91 | 11.87 | 11.82 | 10.61 | 10.23 | 10.20 |
| 6 | 14.12 | 13.94 | 13.17 | 12.60 | 12.07 | 11.70 | 10.94 | 10.25 | 9.98 |
| 7 | 16.23 | 14.97 | 13.91 | 13.42 | 12.34 | 12.19 | 11.14 | 10.54 | 10.45 |
| 8 | 15.01 | 14.53 | 13.62 | 13.00 | 12.30 | 11.98 | 11.25 | 10.55 | 10.41 |
| 9 | 13.20 | 13.57 | 12.93 | 12.87 | 11.97 | 11.96 | 10.91 | 10.62 | 10.63 |
| 10 | 15.06 | 14.68 | 13.69 | 13.13 | 12.44 | 12.06 | 11.44 | 10.62 | 10.38 |

NOTE.—Table 2 is published in its entirety in the electronic edition of the *Astrophysical Journal Supplement*. A portion is shown here for guidance regarding its form and content.

[a] The near-infrared magnitudes for these two galaxies are likely to be overestimated because of their large extent, preventing accurate sky subtraction; see § 2.1 for details.

TABLE 3

2.1″ Aperture Magnitudes for Coma Objects

| ID (Table 1) | *U* | *B* | *V* | *R* | *I* | *z* | *J* | *H* | *K* |
|---|---|---|---|---|---|---|---|---|---|
| 1[a] | 16.98 | 16.43 | 15.31 | 14.69 | 13.98 | 13.95 | 12.88 | 12.12 | 11.85 |
| 2 | 14.15 | 14.16 | 13.39 | 13.46 | 12.25 | 12.36 | 10.70 | 10.20 | 10.55 |
| 3[a] | 17.80 | 17.30 | 16.19 | 15.58 | 14.88 | 14.57 | 13.77 | 12.99 | 12.76 |
| 4 | 13.84 | 14.06 | 13.46 | 13.51 | 12.29 | 12.42 | 10.96 | 10.54 | 10.65 |
| 5 | 14.92 | 14.48 | 13.63 | 13.54 | 12.38 | 12.48 | 10.94 | 10.57 | 10.63 |
| 6 | 17.62 | 17.30 | 16.23 | 15.56 | 14.86 | 14.63 | 13.75 | 12.98 | 12.73 |
| 7 | 16.39 | 15.30 | 14.19 | 13.82 | 12.70 | 12.69 | 11.42 | 10.85 | 10.90 |
| 8 | 17.88 | 17.31 | 16.25 | 15.62 | 14.92 | 14.69 | 13.72 | 12.98 | 12.72 |
| 9 | 13.63 | 14.12 | 13.46 | 13.54 | 12.44 | 12.54 | 11.22 | 10.88 | 11.06 |
| 10 | 16.99 | 16.57 | 15.52 | 14.91 | 14.23 | 13.92 | 13.01 | 12.26 | 12.02 |

Note.—Table 3 is published in its entirety in the electronic edition of the *Astrophysical Journal Supplement*. A portion is shown here for guidance regarding its form and content.

[a] The near-infrared magnitudes for these two galaxies are likely to be overestimated because of their large extent, preventing accurate sky subtraction; see § 2.1 for details.

TABLE 4

4.2″ Aperture Magnitudes for Coma Objects

| ID (Table 1) | *U* | *B* | *V* | *R* | *I* | *z* | *J* | *H* | *K* |
|---|---|---|---|---|---|---|---|---|---|
| 1[a] | 15.92 | 15.38 | 14.25 | 13.65 | 12.93 | 12.73 | 11.82 | 11.06 | 10.81 |
| 2 | 14.03 | 13.87 | 12.88 | 12.69 | 11.72 | 11.71 | 10.25 | 9.66 | 9.91 |
| 3[a] | 16.65 | 16.15 | 15.04 | 14.44 | 13.73 | 13.42 | 12.63 | 11.85 | 11.62 |
| 4 | 13.70 | 13.68 | 12.94 | 12.72 | 11.93 | 11.80 | 10.77 | 10.33 | 10.37 |
| 5 | 14.80 | 14.29 | 13.34 | 12.95 | 12.00 | 11.95 | 10.73 | 10.31 | 10.33 |
| 6 | 16.88 | 16.56 | 15.48 | 14.82 | 14.10 | 13.88 | 13.01 | 12.27 | 11.98 |
| 7 | 16.27 | 15.18 | 14.03 | 13.53 | 12.47 | 12.35 | 11.26 | 10.65 | 10.57 |
| 8 | 16.94 | 16.40 | 15.34 | 14.72 | 14.01 | 13.77 | 12.86 | 12.11 | 11.87 |
| 9 | 13.43 | 13.82 | 13.07 | 13.02 | 12.13 | 12.12 | 11.03 | 10.72 | 10.72 |
| 10 | 16.20 | 15.78 | 14.73 | 14.15 | 13.46 | 13.14 | 12.31 | 11.58 | 11.38 |

Note.—Table 4 is published in its entirety in the electronic edition of the *Astrophysical Journal Supplement*. A portion is shown here for guidance regarding its form and content.

[a] The near-infrared magnitudes for these two galaxies are likely to be overestimated because of their large extent, preventing accurate sky subtraction; see § 2.1 for details.

TABLE 5

6.2″ Aperture Magnitudes for Coma Objects

| ID (Table 1) | *U* | *B* | *V* | *R* | *I* | *z* | *J* | *H* | *K* |
|---|---|---|---|---|---|---|---|---|---|
| 1[a] | 15.47 | 14.86 | 13.70 | 13.10 | 12.47 | 12.12 | 11.37 | 10.61 | 10.34 |
| 2 | 13.88 | 13.65 | 12.79 | 12.65 | 11.57 | 11.54 | 10.12 | 9.52 | 9.76 |
| 3[a] | 16.12 | 15.55 | 14.39 | 13.80 | 13.19 | 12.78 | 12.10 | 11.33 | 11.09 |
| 4 | 13.52 | 13.48 | 12.88 | 12.75 | 11.79 | 11.70 | 10.65 | 10.23 | 10.25 |
| 5 | 14.69 | 14.09 | 13.20 | 12.91 | 11.87 | 11.82 | 10.61 | 10.24 | 10.21 |
| 6 | 16.70 | 16.25 | 15.10 | 14.43 | 13.78 | 13.45 | 12.65 | 11.94 | 11.62 |
| 7 | 16.23 | 15.00 | 13.91 | 13.41 | 12.35 | 12.19 | 11.14 | 10.55 | 10.45 |
| 8 | 16.51 | 15.89 | 14.81 | 14.20 | 13.58 | 13.25 | 12.45 | 11.70 | 11.46 |
| 9 | 13.20 | 13.58 | 12.93 | 12.87 | 11.98 | 11.96 | 10.91 | 10.63 | 10.64 |
| 10 | 15.84 | 15.34 | 14.31 | 13.73 | 13.09 | 12.72 | 11.97 | 11.26 | 11.06 |

Note.—Table 5 is published in its entirety in the electronic edition of the *Astrophysical Journal Supplement*. A portion is shown here for guidance regarding its form and content.

[a] The near-infrared magnitudes for these two galaxies are likely to be overestimated because of their large extent, preventing accurate sky subtraction; see § 2.1 for details.

TABLE 6

8.3″ Aperture Magnitudes for Coma Objects

| ID (Table 1) | *U* | *B* | *V* | *R* | *I* | *z* | *J* | *H* | *K* |
|---|---|---|---|---|---|---|---|---|---|
| 1[a] | 15.24 | 14.61 | 13.56 | 12.96 | 12.25 | 11.97 | 11.14 | 10.39 | 10.12 |
| 2 | 13.87 | 13.64 | 12.78 | 12.63 | 11.55 | 11.52 | 10.11 | 9.51 | 9.75 |
| 3[a] | 15.85 | 15.28 | 14.23 | 13.64 | 12.94 | 12.62 | 11.84 | 11.08 | 10.83 |
| 4 | 13.51 | 13.46 | 12.87 | 12.74 | 11.77 | 11.69 | 10.65 | 10.22 | 10.24 |
| 5 | 14.68 | 14.08 | 13.19 | 12.90 | 11.86 | 11.80 | 10.61 | 10.22 | 10.20 |
| 6 | 16.39 | 15.97 | 14.94 | 14.27 | 13.55 | 13.30 | 12.41 | 11.70 | 11.37 |
| 7 | 16.22 | 15.00 | 13.90 | 13.40 | 12.33 | 12.18 | 11.13 | 10.54 | 10.44 |
| 8 | 16.26 | 15.66 | 14.68 | 14.07 | 13.37 | 13.12 | 12.24 | 11.50 | 11.26 |
| 9 | 13.19 | 13.56 | 12.92 | 12.85 | 11.96 | 11.95 | 10.91 | 10.62 | 10.63 |
| 10 | 15.68 | 15.20 | 14.22 | 13.64 | 12.95 | 12.63 | 11.85 | 11.15 | 10.95 |

Note.—Table 6 is published in its entirety in the electronic edition of the *Astrophysical Journal Supplement*. A portion is shown here for guidance regarding its form and content.

[a] The near-infrared magnitudes for these two galaxies are likely to be overestimated because of their large extent, preventing accurate sky subtraction; see § 2.1 for details.

TABLE 7

10.3″ Aperture Magnitudes for Coma Objects

| ID (Table 1) | *U* | *B* | *V* | *R* | *I* | *z* | *J* | *H* | *K* |
|---|---|---|---|---|---|---|---|---|---|
| 1[a] | 15.09 | 14.48 | 13.43 | 12.83 | 12.12 | 11.85 | 11.01 | 10.25 | 9.99 |
| 2 | 13.87 | 13.63 | 12.77 | 12.61 | 11.54 | 11.50 | 10.11 | 9.53 | 9.74 |
| 3[a] | 15.70 | 15.13 | 14.08 | 13.50 | 12.79 | 12.46 | 11.70 | 10.93 | 10.69 |
| 4 | 13.51 | 13.46 | 12.86 | 12.73 | 11.76 | 11.67 | 10.64 | 10.22 | 10.23 |
| 5 | 14.68 | 14.08 | 13.19 | 12.89 | 11.85 | 11.79 | 10.60 | 10.22 | 10.19 |
| 6 | 16.10 | 15.76 | 14.78 | 14.10 | 13.36 | 13.12 | 12.42 | 11.51 | 11.18 |
| 7 | 16.22 | 14.99 | 13.90 | 13.39 | 12.33 | 12.17 | 11.13 | 10.53 | 10.44 |
| 8 | 16.12 | 15.53 | 14.55 | 13.94 | 13.24 | 12.99 | 12.12 | 11.37 | 11.15 |
| 9 | 13.19 | 13.55 | 12.91 | 12.84 | 11.96 | 11.93 | 10.90 | 10.61 | 10.62 |
| 10 | 15.61 | 15.13 | 14.14 | 13.56 | 12.87 | 12.56 | 11.78 | 11.09 | 10.88 |

Note.—Table 7 is published in its entirety in the electronic edition of the *Astrophysical Journal Supplement*. A portion is shown here for guidance regarding its form and content.

[a] The near-infrared magnitudes for these two galaxies are likely to be overestimated because of their large extent, preventing accurate sky subtraction; see § 2.1 for details.

TABLE 8

$r_1$ Aperture Magnitudes for Coma Objects

| ID (Table 1) | *U* | *B* | *V* | *R* | *I* | *z* | *J* | *H* | *K* |
|---|---|---|---|---|---|---|---|---|---|
| 1[a] | 15.09 | 14.48 | 13.43 | 12.83 | 12.12 | 11.85 | 11.01 | 10.25 | 9.99 |
| 2 | 13.87 | 13.63 | 12.77 | 12.61 | 11.54 | 11.50 | 10.11 | 9.53 | 9.74 |
| 3[a] | 15.70 | 15.13 | 14.08 | 13.50 | 12.79 | 12.46 | 11.70 | 10.93 | 10.69 |
| 4 | 13.51 | 13.46 | 12.86 | 12.73 | 11.76 | 11.67 | 10.64 | 10.22 | 10.23 |
| 5 | 14.68 | 14.08 | 13.19 | 12.89 | 11.85 | 11.79 | 10.60 | 10.22 | 10.19 |
| 6 | 16.10 | 15.76 | 14.78 | 14.10 | 13.36 | 13.12 | 12.24 | 11.51 | 11.18 |
| 7 | 16.22 | 14.99 | 13.90 | 13.39 | 12.33 | 12.17 | 11.13 | 10.53 | 10.44 |
| 8 | 16.12 | 15.53 | 14.55 | 13.94 | 13.24 | 12.99 | 12.12 | 11.37 | 11.15 |
| 9 | 13.19 | 13.55 | 12.91 | 12.84 | 11.96 | 11.93 | 10.90 | 10.61 | 10.62 |
| 10 | 15.61 | 15.13 | 14.14 | 13.56 | 12.87 | 12.56 | 11.78 | 11.09 | 10.88 |

Note.—Table 8 is published in its entirety in the electronic edition of the *Astrophysical Journal Supplement*. A portion is shown here for guidance regarding its form and content.

[a] The near-infrared magnitudes for these two galaxies are likely to be overestimated because of their large extent, preventing accurate sky subtraction; see § 2.1 for details.

TABLE 9
SELECTED COLORS OF COMA GALAXIES

| ID (Table 1) | $H$ | $U-B$ | $U-V$ | $B-V$ | $B-R$ | $V-I$ | $V-K$ | $I-K$ | $J-K$ |
|---|---|---|---|---|---|---|---|---|---|
| 1 | 9.14 | 0.66 | 1.83 | 1.17 | 1.76 | 1.28 | 3.41 | 2.13 | 1.03 |
| 3 | 9.60 | 0.62 | 1.78 | 1.17 | 1.75 | 1.25 | 3.35 | 2.10 | 1.01 |
| 6 | 10.25 | 0.50 | 1.66 | 1.16 | 1.83 | 1.36 | 3.53 | 2.16 | 1.03 |
| 8 | 10.55 | 0.67 | 1.75 | 1.08 | 1.68 | 1.28 | 3.40 | 2.12 | 0.99 |
| 10 | 10.62 | 0.55 | 1.59 | 1.03 | 1.61 | 1.27 | 3.30 | 2.03 | 0.91 |
| 12 | 10.76 | 0.55 | 1.61 | 1.06 | 1.66 | 1.30 | 3.37 | 2.07 | 0.96 |
| 14 | 10.87 | 0.56 | 1.65 | 1.09 | 1.68 | 1.28 | 3.28 | 2.00 | 0.89 |
| 15 | 10.88 | 0.51 | 1.61 | 1.10 | 1.67 | 1.23 | 3.28 | 2.05 | 0.97 |
| 16 | 10.94 | 0.57 | 1.61 | 1.04 | 1.65 | 1.30 | 3.43 | 2.13 | 0.94 |
| 17 | 10.98 | 0.48 | 1.55 | 1.07 | 1.64 | 1.25 | 3.28 | 2.03 | 0.99 |
| 20 | 11.26 | 0.53 | 1.56 | 1.02 | 1.63 | 1.32 | 3.40 | 2.08 | 1.01 |
| 21 | 11.26 | 0.56 | 1.68 | 1.11 | 1.67 | 1.26 | 3.33 | 2.07 | 0.99 |
| 23 | 11.30 | 0.54 | 1.57 | 1.03 | 1.60 | 1.29 | 3.33 | 2.04 | 0.99 |
| 24 | 11.32 | 0.55 | 1.64 | 1.09 | 1.67 | 1.27 | 3.32 | 2.05 | 1.00 |
| 25 | 11.37 | 0.54 | 1.65 | 1.11 | 1.69 | 1.27 | 3.34 | 2.07 | 1.00 |
| 26 | 11.39 | 0.52 | 1.58 | 1.06 | 1.60 | 1.24 | 3.22 | 1.98 | 0.98 |
| 27 | 11.40 | 0.54 | 1.59 | 1.05 | 1.63 | 1.27 | 3.28 | 2.01 | 0.96 |
| 28 | 11.42 | 0.47 | 1.53 | 1.07 | 1.63 | 1.24 | 3.18 | 1.94 | 0.95 |
| 29 | 11.44 | 0.51 | 1.58 | 1.07 | 1.64 | 1.24 | 3.25 | 2.01 | 0.94 |
| 30 | 11.44 | 0.45 | 1.49 | 1.05 | 1.61 | 1.21 | 3.14 | 1.93 | 0.96 |

NOTE.—Table 9 is published in its entirety in the electronic edition of the *Astrophysical Journal Supplement*. A portion is shown here for guidance regarding its form and content.

$I$, and 1800 s in $z$. Reduction was carried out in the standard way for these images. The $I$ and $z$ images were obtained in photometric conditions and calibrated using standards of observations by Landolt (1992) and Thuan & Gunn (1976). The $z$-band transformations are judged to be accurate to only $\pm 0.15$ mag. Nonphotometric data in $B$, $V$, and $R$ were recalibrated using observations of a $9.7' \times 9.7'$ portion of the Coma field and of 25 standards obtained in photometric conditions with the COSMIC instrument (using a $2048^2$ CCD with $0.2846''$ pixels) on the Palomar 200 inch telescope on 1995 February 2. The $U$-band images from Kitt Peak were calibrated by matching photometry in large apertures on galaxies whose $U$ photometry was published by Bower et al. (1992). The optical and infrared images were registered to a common coordinate system, degraded to the same resolution ($0.6845''$ pixel$^{-1}$) and blurred to the seeing of the worst image ($1.7''$ FWHM). The reduced and calibrated FITS files for the optical and infrared mosaics will be made publicly available through the Data Products Program.

### 2.3. *Photometry*

We used FOCAS (Jarvis & Tyson 1981; Valdes 1982) on the $J$ and $H$ images to produce two independent catalogs. The detection limit was chosen to be 3.5 $\sigma$ above the sky level in an area equal to the point-spread function (PSF) disk. The two catalogs were position matched to eliminate false detections. Only objects present in both catalogs were accepted in the final catalog (under the assumption that Coma galaxies have similar infrared colors so that the $J$ and $H$ images reach similar depths).

Astrometry for cataloged objects was determined using bright galaxies to establish an initial solution using the IRAF task `ccmap`. This solution was then used to identify $\sim$50 objects in the catalog with $H < 15$ that were classified as stars by Lobo et al. (1997). These stars were then used to determine the final astrometric solution, which had residual errors of $0.4''$. Cataloged objects were identified with objects in existing catalogs if their positions agreed to within $3''$, using NED and Lobo et al. (1997).

The angular size of galaxies in the catalog varies widely, requiring the use of an adaptive aperture size for photometry.

TABLE 10
PARAMETERS FOR ERRORS IN $6.2''$ APERTURE

| Band | $a$ | $b$ |
|---|---|---|
| $U$ | 0.582 | 13.94 |
| $B$ | 0.620 | 15.02 |
| $V$ | 0.715 | 16.25 |
| $R$ | 0.647 | 14.42 |
| $I$ | 0.781 | 15.73 |
| $z$ | 0.715 | 14.61 |
| $J$ | 0.909 | 16.40 |
| $H$ | 0.776 | 13.65 |
| $K$ | 0.805 | 13.81 |

TABLE 11
COMPARISON WITH PREVIOUS WORK

| Band | $\Delta$mag (This Work) (mag) | $\sigma$ | Reference |
|---|---|---|---|
| $U$ | 0.028 | 0.037 | BLE92 |
| | 0.156 | 0.059 | Strom & Strom (1978) |
| $B$ | 0.028 | 0.047 | Strom & Strom (1978) |
| | 0.016 | 0.107 | Doi et al. (1995) |
| $V$ | 0.024 | 0.020 | BLE92 |
| | 0.019 | 0.042 | Strom & Strom (1978) |
| | 0.078 | 0.104 | Lobo et al. (1997) |
| $R$ | −0.261 | 0.108 | Strom & Strom (1978) |
| | −0.020 | 0.088 | Bernstein et al. (1995) |
| | −0.210 | 0.134 | Jørgensen & Franx (1994) |
| | −0.213 | 0.023 | Secker et al. (1997) |
| $J$ | −0.019 | 0.049 | BLE92 |
| | −0.021 | 0.046 | PFA79 |
| $H$ | 0.010 | 0.051 | BLE92 |
| | −0.002 | 0.047 | PFA79 |
| $K$ | −0.012 | 0.041 | BLE92 |
| | −0.009 | 0.049 | PFA79 |

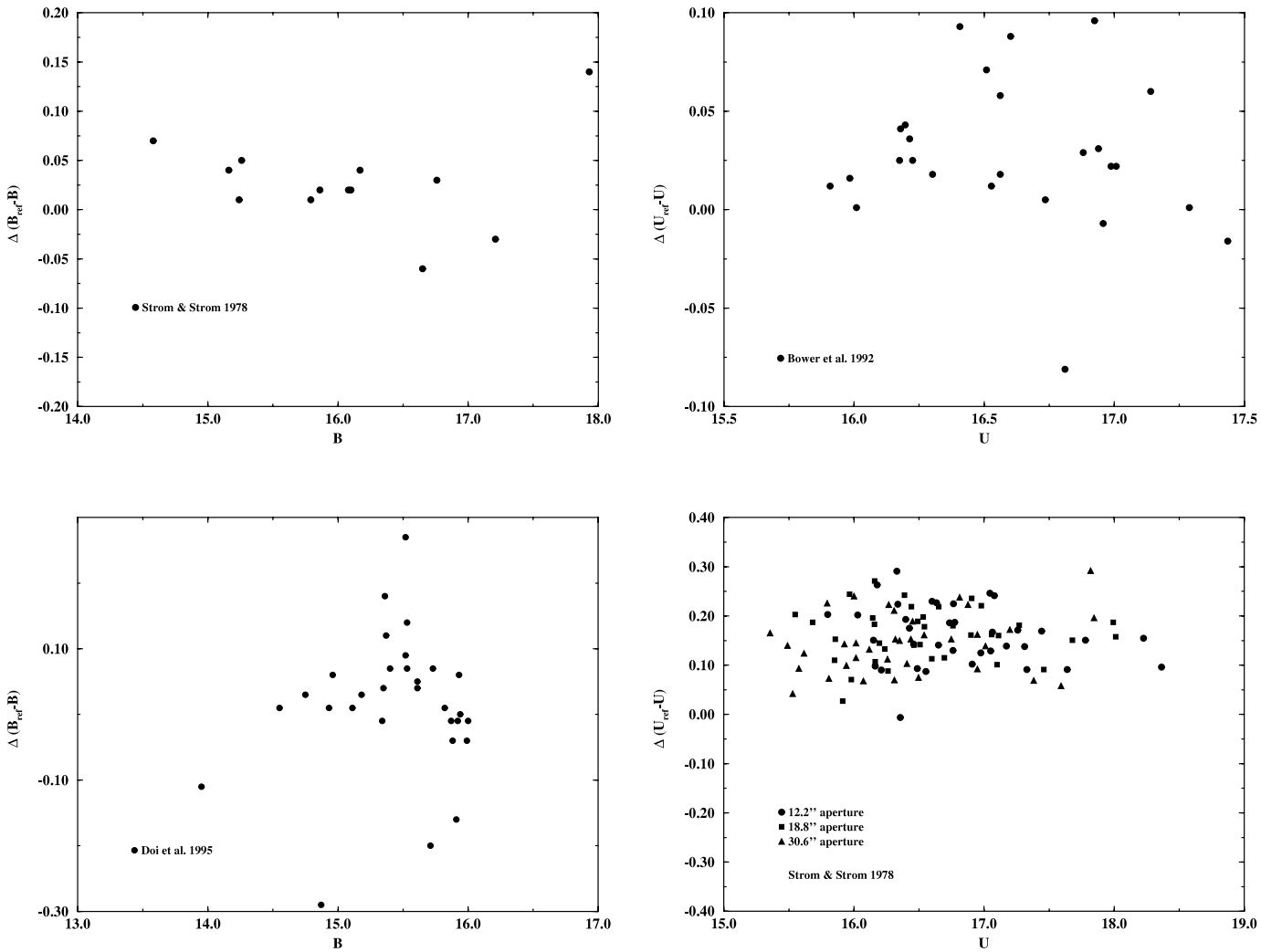


FIG. 2.—Comparison of our photometry with reference photometry (see Table 11). The sources for the comparisons are indicated in the figure panel.

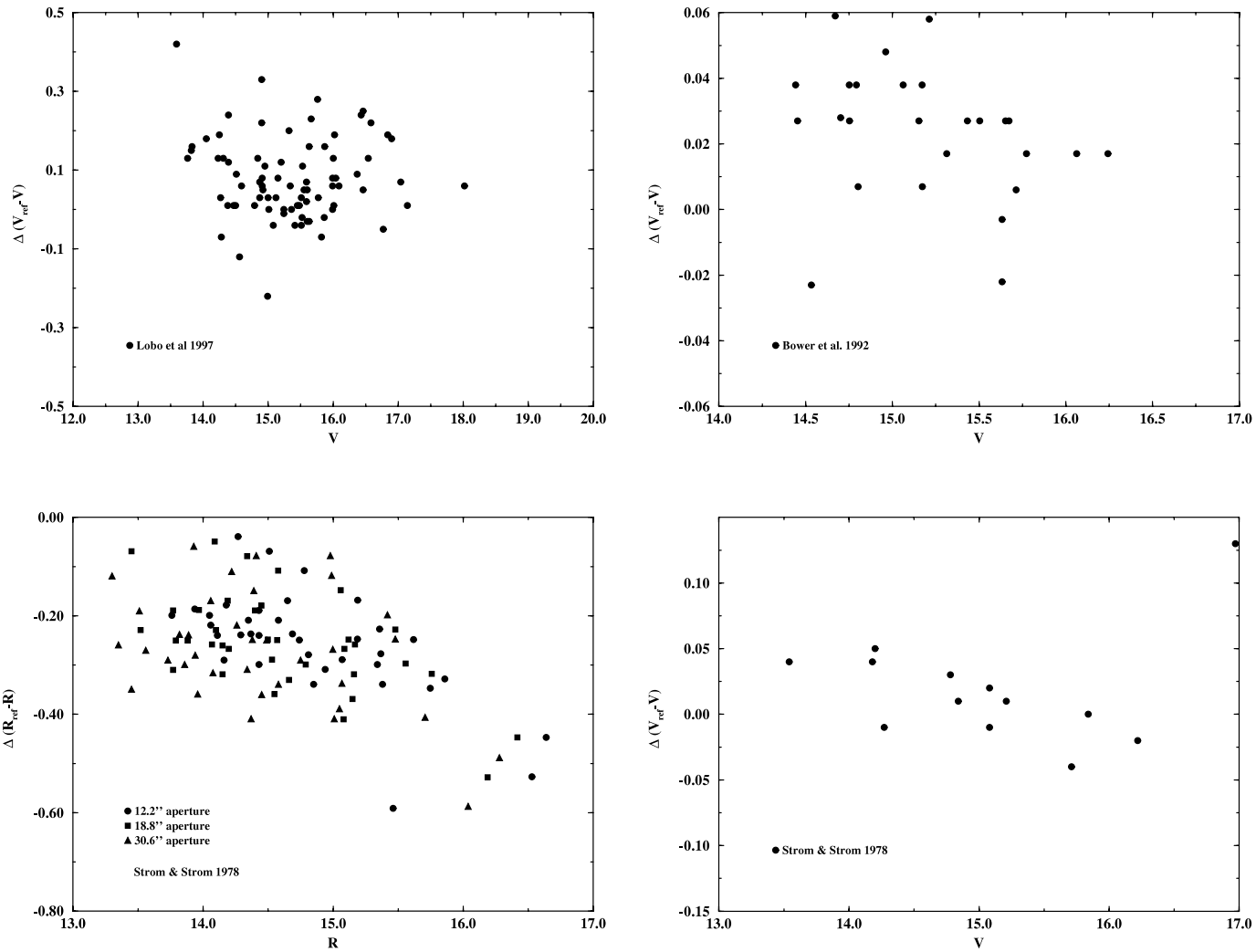


FIG. 2—*Continued*

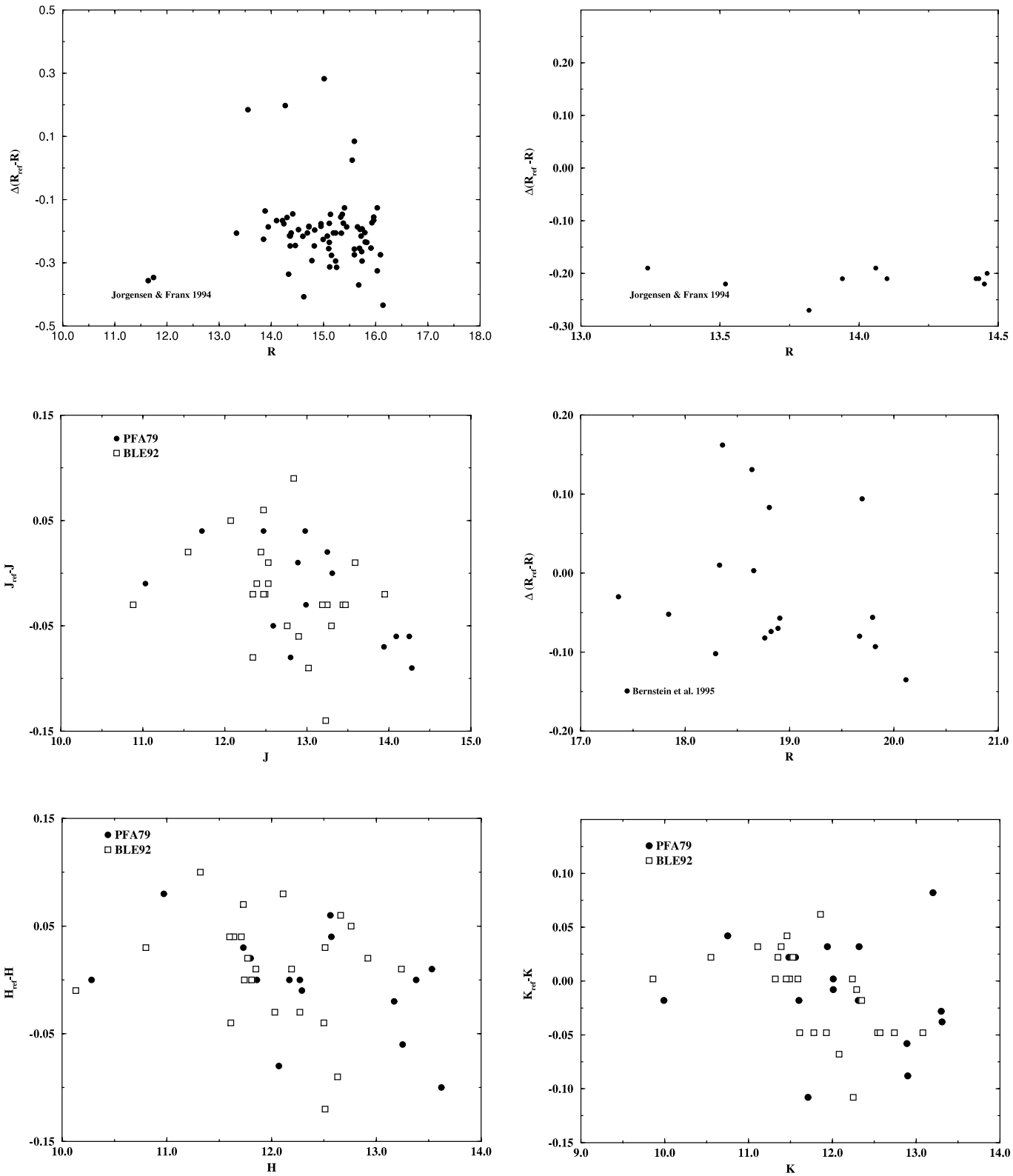


FIG. 2—*Continued*

Simple single-aperture photometry would introduce excessive noise for faint objects if the aperture used is too large or omit substantial light from larger galaxies in the opposite case. An additional problem is deciding which light should be associated with which galaxy, particularly in the central regions where galaxies are clearly overlapping.

Software designed for analysis of faint galaxies in moderately crowded fields was kindly provided to us by L. Infante and C. J. Pritchet of the University of Victoria (Infante 1987), containing provisions for a (simple) excision of contaminating objects. For each object Kron (1980) image moments $r_1$ and $r_{-2}$ were computed, where $r_1$ is the first moment of the light profile and hence a measure of galaxy size, while $r_{-2}$ measures compactness and is defined by the deviation of the area of the galaxy under the light profile from a PSF.

Photometry in apertures of radius $2r_1$ is found to enclose most (>96%) of the total light (Infante 1987). These apertures vary from object to object and may change from band to band. From simulations with $r^{1/4}$ profiles, it was found necessary to ensure that the measurement aperture within which $r_1$ was determined had a radius at least 5 times larger than $r_1$ to achieve a convergent value of $r_1$. For some of the brightest and largest objects this was impractical. For the brightest 10 galaxies 50 kpc (diameter) apertures were adopted to approximate total magnitudes. Model light profiles were fit to the brightest two galaxies (Nos. 1 and 3) and to the brightest star and the resulting models subtracted before measuring photometry on the remaining objects. For the galaxies with $11 \lesssim H \lesssim 13$ fixed 30 kpc (diameter) apertures were used (for consistency with Stanford et al. 1995, 1998). For fainter objects $2r_1$ apertures were used. These choices were found to be best in terms of photometric accuracy, stability, and noise.

Star-galaxy separation was determined using the classification by Lobo et al. (1997), which uses optical data taken in good seeing, and reaches $V = 22.5$. The only objects identified in the present catalog not found in other catalogs were Nos. 66, 225, and 711, all of which were outside the Lobo et al. (1997) area (which does not cover R.A. $> 13^{\rm h}00^{\rm m}30^{\rm s}$ and decl. $< 27^\circ49'13''$ in our survey area). Star-galaxy separation in the region not surveyed by Lobo et al. (1997) was determined using the $r_{-2}$ compactness parameter (Kron 1980).

## 3. PHOTOMETRIC CATALOG

Table 1 presents our catalog of objects. In column (1) we show our ID number, in order of decreasing $H$ luminosity (see discussion for Table 2 below). Equatorial coordinates (J2000.0) are given in columns (2) and (3). Column (4) shows our $H$ magnitude. Column (5) gives the classification as star or galaxy, or if available its morphological type taken from Dressler (1980), Rood & Baum (1967), Caldwell et al. (1993), Graham & Guzman (2003), or the classification shown in the NASA Extragalactic Database (NED) in a few cases (mostly for faint galaxies for which the source of the NED classification was unclear). The source for the morphological class is in column (6). Redshifts, compiled from the best values (lowest stated error) in NED, are in column (7). The sources for the redshifts are given in column (8). Identification numbers from the Godwin et al. (1983, hereafter GMP83) catalog are given in column (9). Cross-identifications from the NGC, IC, Rood & Baum (1967), and Dressler (1980) catalogs are shown in column (10). Notes on some objects are in column (11). We present the first lines of this table in the printed version, the remainder being available in electronic format.

Table 2 summarizes our estimates of total magnitude in all the bands. The layout of this table is repeated for all photometry tables to follow: in column order we give our ID, $U$, $B$, $V$, $R$, $I$, $z$, $J$, $H$, and $K$. Again, we show the first few lines of this table and make the rest available electronically.

TABLE 12

*UBVRIzJHK$_s$* Band Response Functions

| Wavelength (Å) | Throughput (%) |
|---|---|
| *U* Band | |
| 3050 | 0 |
| 3100 | 0.000117987 |
| 3150 | 0.0010573 |
| 3200 | 0.00422111 |
| 3250 | 0.0142508 |
| 3350 | 0.0773872 |
| 3400 | 0.137695 |
| 3450 | 0.223221 |
| 3500 | 0.334892 |
| 3550 | 0.475813 |

Note.—Table 12 is published in its entirety in the electronic edition of the *Astrophysical Journal Supplement*. A portion is shown here for guidance regarding its form and content.

Tables 3–8 show the same information for apertures of 2.1″, 4.2″, 6.2″, 8.3″, 10.3″ (radius), and $r_1$. The aperture magnitudes (50 and 30 kpc) for the brightest objects are reported in Table 2. Finally, by way of example, we show total $H$ magnitudes and 6.2″ aperture colors for eight colors of common astrophysical interest in Table 9 (first few lines in the printed version, with the rest of the table being made available electronically).

Magnitude errors were estimated via bootstrap simulations. Representative galaxies over a 6 mag range in each band were replicated 20 times on a grid in the image, and their magnitudes extracted. At a total magnitude of $H \sim 15$ a signal-to-noise ratio of 5 was achieved, consistent with expectations. Table 10 gives functional forms for the variations of the error with magnitude in the 6.2″ aperture, of the form $\sigma_{\rm band} = \exp[a\times({\rm mag}) - b]$, where "mag" is the magnitude in the filter "band." Simulations in which galaxies with known magnitudes and $r_1$ were replicated and added to the data show that the catalog is at least 90% complete to $H = 16.5$ for $r_1 \leq 2.05''$ and at least 80% complete to $H = 16$ for $r_1 \leq 4.1''$.

### 3.1. *Comparison with Previous Photometry*

Table 11 compares our photometry to previous work. Where possible, we derived magnitudes in exactly the same apertures as the comparison measurements. The only exceptions are for Doi et al. (1995) and Lobo et al. (1997), who quote isophotal magnitudes. For these we computed magnitudes in a circular aperture having radius equivalent to the semimajor axis of the limiting isophote. Figure 2 shows the comparisons between the reference photometry and our data.

Our photometry is generally within 2%–3% of the reference magnitudes. Small differences in the central filter bandpass and calibration errors can easily account for discrepancies at a few percent level. However, we find a difference of 0.16 mag between our $U$-band data (and those of Bower et al. 1992) and the photographic photometry of Strom & Strom (1978). We also find a difference of 0.26 mag between our work and Strom & Strom (1978) in $R$ and of 0.21 mag between this work and the Cousins $R$ data of Secker et al. (1997) and Jørgensen & Franx (1994). Our photometry agrees with the Harris $R$ magnitudes of Bernstein et al. (1995) taken with the same filter/detector combination, within 2%.

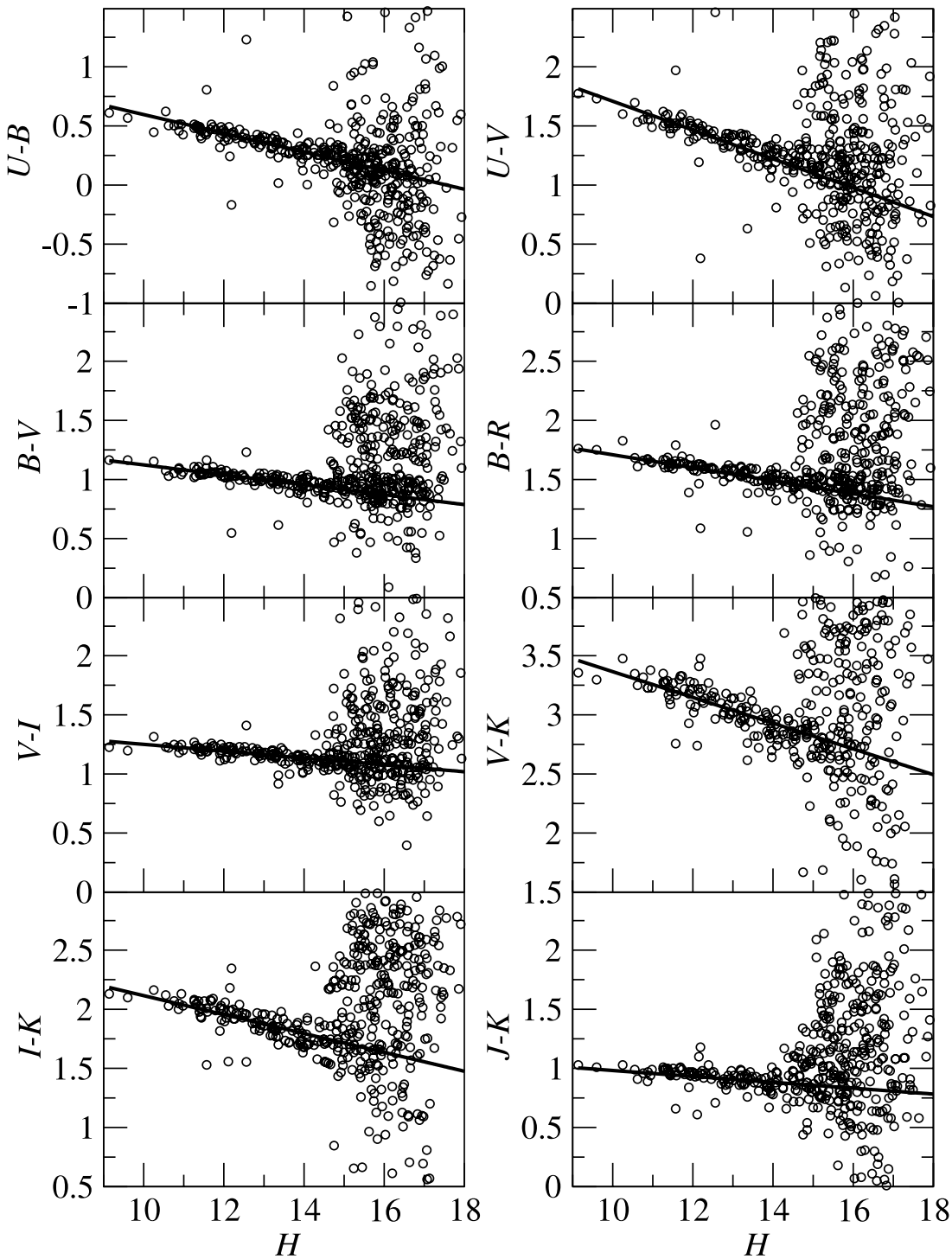


FIG. 3.—CMRs for the eight representative colors tabulated in Table 9. The straight lines show the best fits, whose slopes, intercepts, and scatter are tabulated in Table 13.

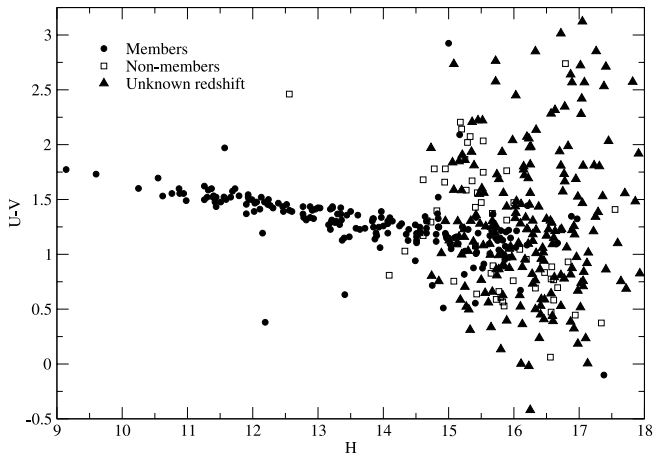


FIG. 4.—Expanded plot for $U - V$ vs. $H$, showing spectroscopic members, nonmembers, and objects with unknown redshifts.

We convolve the spectral energy distribution of a typical early-type galaxy, with the sensitivity function for the detector used and the filter bandpass, to derive predicted offsets in magnitude between our data and the comparison work used. In the $R$ band, we find that the predicted difference between our photometry and the work of Jørgensen & Franx (1994) and Secker et al. (1997) is $-0.172$ mag, in good agreement with the $-0.210$ that we measure. For the 127-04 emulsion and RG610 filter used by Strom & Strom (1978) we find a discrepancy of $-0.26$, identical to the observed value. Similarly, for the IIIa-J emulsion and UG-2 filter used by Strom & Strom (1978) in the $U$, we predict a difference of 0.188 mag, which compares well with the 0.156 mag found. Applying these corrections, our data lie within a few percent of all previous photometry. When we compare with Lobo et al. (1997) we also find a difference of 0.08 mag in the $V$ band: however, the different photometric methods employed (isophotal apertures vs. circular ones) are at least as important as differences in filter bandpasses and detectors.

To facilitate comparisons to our photometry, we provide the response functions for our bands in Table 12, including the effects of filter and atmospheric transmission, and quantum efficiency.

## 4. THE COLOR-MAGNITUDE RELATION OF EARLY-TYPE GALAXIES IN COMA

As an example application of this data set we study the color-magnitude relation of early-type (E or S0) galaxies and its intrinsic scatter, for the eight colors shown in Table 9, using the 111 galaxies brighter than $H = 14.5$ for which we have a complete sample of cluster members. Morphologies for these galaxies are taken from the compilation of Dressler (1980) or Rood & Baum (1967) in order of preference. Only seven of these 111 galaxies do not have a morphological classification from these sources, and we accordingly do not use them for computation of CMRs and scatter.

Scodeggio (2001) has suggested that the actual slope of the CMR is much flatter than measured here (and elsewhere) and that this is due to the use of a fixed aperture for all galaxies rather than an adaptive aperture based on the structural parameters of each galaxy (e.g., using the half-light radius). Because galaxies have internal color gradients, a fixed aperture samples more metal poor populations for the fainter galaxies, thus steepening the color-magnitude trend (which is largely a mass-metallicity trend; Trager et al. 2000; Terlevich et al. 2001).

To examine the effect of color gradients within galaxies on the derived CMRs, we measured and fit the $U - V$ versus $V$ CMR using a series of fixed circular apertures with radii ranging from $2.1''$ to $10.3''$. We also used apertures with radii $r_1$ and $2r_1$, where $r_1$ is the first moment of the light profile (Kron 1980) and is calculated for each galaxy. The $r_1$ and $2r_1$ apertures should not be affected by the $1.7''$ FWHM seeing, as they are generally considerably larger. The intercept of the CMR is redder for smaller apertures, as expected given the general sense of color gradients that are observed within elliptical galaxies. The slope, however, changes only slightly with aperture size, from $-0.128$ for the smallest aperture to $-0.085$ for $r = 2r_1$. By contrast, Scodeggio (2001) finds an essentially flat relation when measured within $r_e$ in $U - V$ versus $V$. However, our findings are consistent with the mild color gradients observed for E/S0 galaxies in nearby clusters by Tamura & Ohta (2003).

Although it is important to remember that any derived CMR does depend on the apertures used for the photometry, particularly in its intercept, our basic results concerning the slope and scatter of the CMR are insensitive to the aperture size used, and we therefore restrict our attention to the fixed $6.2''$ radius apertures for the remainder of this paper.

Figure 3 shows the CMRs and best linear regression fits for the colors listed in Table 9 versus total $H$-band magnitude. (For reference, $L^*$ in the $H$ band is 11.13; De Propris et al. 1998.) In Figure 4 we show one of these CMRs using different symbols for members and nonmembers (the plots in Fig. 3 are too compressed to show these clearly).

The slope and intercepts of these fits are shown in Table 13. The intrinsic scatter, also tabulated in Table 13, is calculated using the bootstrap method of Stanford et al. (1995, 1998). One can see that the slope flattens for colors redder than $V$ and that the intrinsic scatter is approximately constant for colors that are equally spaced in (logarithmic) wavelength, suggesting that the relation is indeed driven primarily by metal abundance and that the majority of the stellar populations were formed at early epochs (this is due to the fact that for old stellar populations the only age- and

TABLE 13
COLOR-MAGNITUDE RELATIONS AND SCATTER

| Color | Slope | Intercept | Scatter (Measured) | Photometric Error | Intrinsic Scatter |
|---|---|---|---|---|---|
| $U - B$ | $-0.079 \pm 0.007$ | $1.386 \pm 0.089$ | $0.041 \pm 0.005$ | $0.016 \pm 0.002$ | $0.038 \pm 0.006$ |
| $U - V$ | $-0.122 \pm 0.010$ | $2.929 \pm 0.123$ | $0.050 \pm 0.004$ | $0.016 \pm 0.002$ | $0.047 \pm 0.004$ |
| $B - V$ | $-0.042 \pm 0.004$ | $1.543 \pm 0.049$ | $0.028 \pm 0.004$ | $0.008 \pm 0.001$ | $0.027 \pm 0.004$ |
| $B - R$ | $-0.055 \pm 0.006$ | $2.259 \pm 0.074$ | $0.030 \pm 0.004$ | $0.008 \pm 0.001$ | $0.029 \pm 0.004$ |
| $V - I$ | $-0.029 \pm 0.005$ | $1.540 \pm 0.066$ | $0.033 \pm 0.003$ | $0.010 \pm 0.001$ | $0.031 \pm 0.003$ |
| $V - K$ | $-0.109 \pm 0.017$ | $4.455 \pm 0.209$ | $0.074 \pm 0.010$ | $0.015 \pm 0.002$ | $0.072 \pm 0.010$ |
| $I - K$ | $-0.080 \pm 0.013$ | $2.915 \pm 0.164$ | $0.066 \pm 0.009$ | $0.012 \pm 0.002$ | $0.065 \pm 0.009$ |
| $J - K$ | $-0.025 \pm 0.009$ | $1.232 \pm 0.111$ | $0.036 \pm 0.006$ | $0.016 \pm 0.002$ | $0.025 \pm 0.007$ |

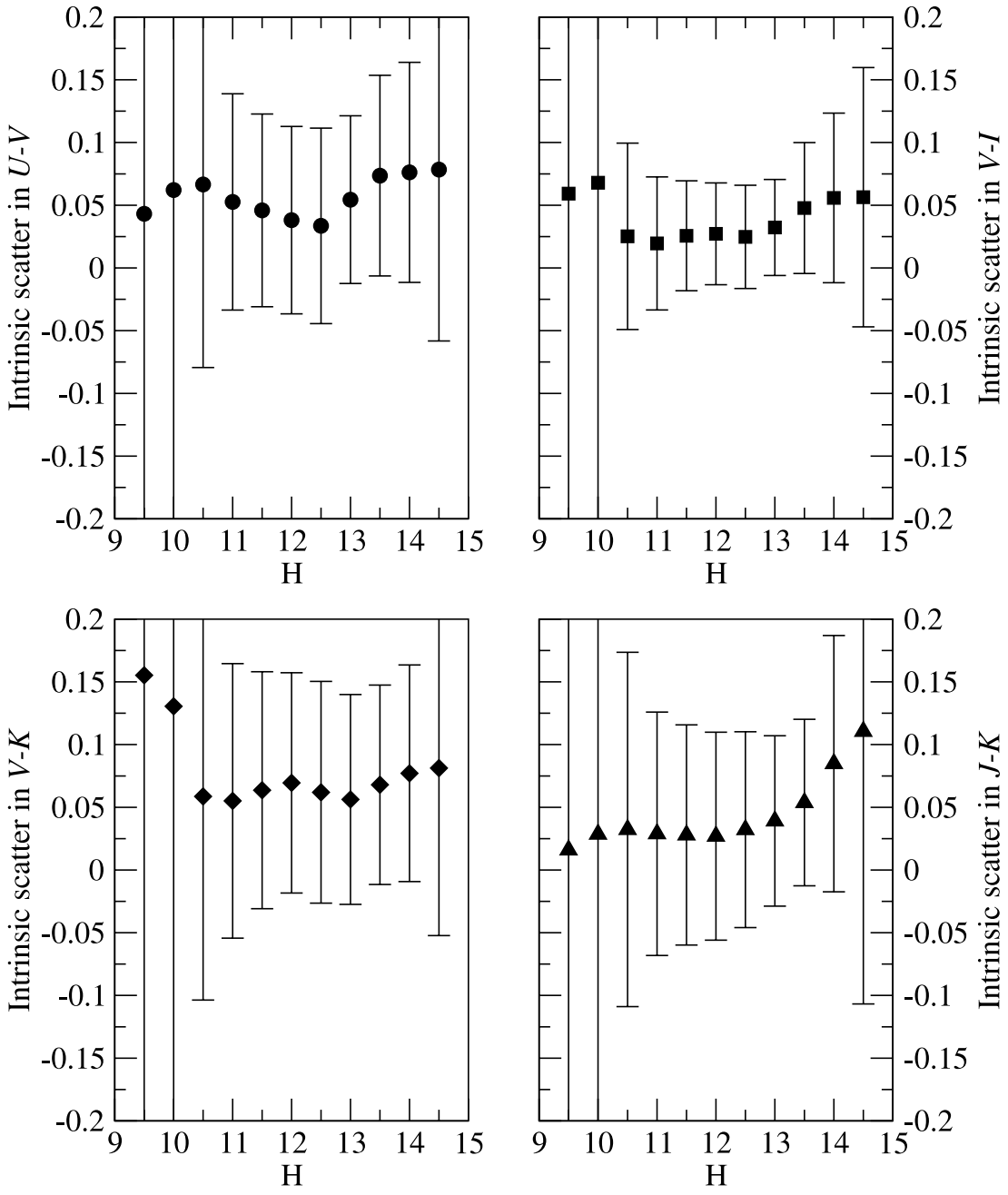


FIG. 5.—Intrinsic scatter about the CMR as a function of *H*-band magnitude, for four colors.

metallicity-sensitive index lies in the region of the 4000 Å break and the magnesium complex; see Kodama & Arimoto 1997; Vazdekis et al. 2001).

It is also interesting to calculate how the intrinsic scatter varies with galaxy *H*-band luminosity (i.e., stellar mass): Figure 5 shows the variation of the intrinsic scatter in 0.5 mag bins for four colors. We see no evidence that the intrinsic scatter varies with galaxy luminosity (this can also be appreciated from Fig. 3, where the CMR does not appear to spread at faint luminosities).

The existence of a color-magnitude relation is ascribed to a relation between galaxy mass and metallicity, which is suitably explained by models of monolithic collapse followed by fast winds. The small scatter about the relation implies that most of the stellar populations must be quite old and that the timescale for galaxy formation is relatively short, while few mergers may have occurred since early epochs (Bower et al. 1992, 1998). Our observations confirm the small scatter seen by Bower but also show that the small scatter extends to fainter elliptical galaxies ($\sim L^* + 3$). This suggests that the stellar populations of all cluster early-type galaxies, irrespective of mass, may have formed rapidly and at high redshift, and that the CMR was formed at an early epoch. Indeed, a mature relation is already observed in the $z = 0.83$ cluster MS 1054−0321 (Andreon 2006). A similar conclusion was also reached by Andreon et al. (2006) on the basis of their thin CMR in Abell 1185. The fact that the intrinsic scatter of the CMR is small for both bright and faint galaxies implies that all red sequence galaxies, irrespective of mass, have undergone a rapid star formation history, in contrast with evidence for

"downsizing" among the faint field (and high redshift) galaxy population (Heavens et al. 2004) or for a truncated sequence at higher redshifts (De Lucia et al. 2004).

We thank George Jacoby for taking the optical data for us. We also thank the anonymous referee for a very helpful report that helped make the paper better. Portions of this research were carried out at Jet Propulsion Laboratory, California Institute of Technology, under a contract with NASA. The work of S. A. S. was performed under the auspices of the US Department of Energy, National Nuclear Security Administration, by the University of California, Lawrence Livermore National Laboratory, under contract W-7405-Eng-48.

REFERENCES

Adami, C., Ulmer, M. P., Durret, F., Nichol, R. C., Mazure, A., Holden, B. P., Romer, A. K., & Savine, C. 2000, A&A, 353, 930
Andreon, S. 2006, MNRAS, 369, 969
Andreon, S., Cuillandre, J.-C., Puddu, E., & Mellier, Y. 2006, MNRAS, 372, 60
Bell, E. F., & de Jong, R. S. 2001, ApJ, 550, 212
Bernstein, G. M., Nichol, R. C., Tyson, J. A., Ulmer, M. P., & Wittman, D. 1995, AJ, 110, 1507
Biviano, A., Durret, F., Gerbal, D., Le Fèvre, O., Lobo, C., Mazure, A., & Slezak, C. 1995, A&AS, 111, 265
Blakeslee, J. P., et al. 2003, ApJ, 596, L143
Bower, R. G., Kodama, T., & Terlevich, A. 1998, MNRAS, 299, 1193
Bower, R. G., Lucey, J. R., & Ellis, R. S. 1992, MNRAS, 254, 601
Caldwell, N., Rose, J. A., Sharples, R. M., Ellis, R. S., & Bower, R. G. 1993, AJ, 106, 473
Casoli, F., Dickey, J., Kazes, I., Boselli, A., Gavazzi, G., & Jore, K. 1996, A&AS, 116, 193
Castander, F., et al. 2001, AJ, 121, 2331
Colless, M. M., & Dunn, A. M. 1996, ApJ, 458, 435
De Lucia, G., et al. 2004, ApJ, 610, L77
De Propris, R., Eisenhardt, P. R., Stanford, S. A., & Dickinson, M. 1998, ApJ, 503, L45
De Propris, R., Stanford, S. A., Eisenhardt, P. R., Dickinson, M., & Elston, R. 1999, AJ, 118, 719
Doi, M., Fukugita, M., Okamura, S., & Turner, E. L. 1995, AJ, 109, 1490
Dressler, A. 1980, ApJS, 42, 565
Dressler, A., & Shectman, S. A. 1988, AJ, 95, 284
Edwards, S. A., Colless, M., Bridges, T. J., Carter, D., Mobasher, B., & Poggianti, B. M. 2002, ApJ, 567, 178
Eggen, O. J., Lynden-Bell, D., & Sandage, A. 1962, ApJ, 136, 748
Elias, J. H., Frogel, J. A., Matthews, K., & Neugebauer, G. 1982, AJ, 87, 1029
Ellis, S. C., Jones, L. R., Donovan, D., Ebeling, H., & Khosroshahi, H. G. 2006, MNRAS, 368, 769
Gavazzi, G., Pierini, D., & Boselli, A. 1996, A&A, 312, 397
Godwin, J. G., Metcalfe, N., & Peach, J. V. 1983, MNRAS, 202, 113
Graham, A. W., & Guzman, R. 2003, AJ, 125, 2936
Haynes, M. P., Giovanelli, R., Herter, T., Vogt, N. P., Freudling, W., Maia, M. A. G., Salzer, J. J., & Wegner, G. 1997, AJ, 113, 1197
Heavens, A., Panter, B., Jimenez, R., & Dunlop, J. 2004, Nature, 428, 625
Holden, B. P., Stanford, S. A., Eisenhardt, P. R., & Dickinson, M. 2004, AJ, 127, 2484
Holden, B. P., et al. 2006, ApJ, 642, L123
Infante, L. 1987, A&A, 183, 177
Jarvis, J. F., & Tyson, J. A. 1981, AJ, 86, 476
Jørgensen, I., & Franx, M. 1994, ApJ, 433, 553
Kajisawa, M., et al. 2000, PASJ, 52, 61
Kaviraj, S., Devriendt, J. E. G., Ferreras, I., & Yi, S. K. 2005, MNRAS, 360, 60
Kodama, T., & Arimoto, N. 1997, A&A, 320, 41
Kron, R. G. 1980, ApJS, 43, 305
Landolt, A. U. 1992, AJ, 104, 340
Lidman, C., Rosati, P., Demarco, R., Nonino, M., Mainieri, V., Stanford, S. A., & Toft, S. 2004, A&A, 416, 829
Lobo, C., Biviano, A., Durret, F., Gerbal, D., Le Fèvre, O., Mazure, A., & Slezak, E. 1997, A&AS, 122, 409
Lopez-Cruz, O., Barkhouse, W., & Yee, H. K. C. 2004, ApJ, 614, 679
Matkovic, A., & Guzman, R. 2005, MNRAS, 362, 289
McIntosh, D. H., Zabludoff, A. I., Rix, H.-W., & Caldwell, N. 2005, ApJ, 619, 193
Mei, S., et al. 2006a, ApJ, 639, 81
———. 2006b, ApJ, 644, 759
Mobasher, B., et al. 2001, ApJS, 137, 279
Moore, S. A. W., Lucey, J. R., Kuntschner, H., & Colless, M. M. 2002, MNRAS, 336, 382
Müller, K. R., Wegner, G., Raychaudhury, S., & Freudling, W. 1999, A&AS, 140, 327
Persson, S. E., Frogel, J. A., & Aaronson, M. 1979, ApJS, 39, 61
Renzini, A. 2006, ARA&A, 44, 141
Rood, H. J., & Baum, W. A. 1967, AJ, 72, 398
Sandage, A., & Visvanathan, N. 1978, ApJ, 223, 707
Scodeggio, M. 2001, AJ, 121, 2413
Secker, J., Harris, W. E., & Plummer, J. D. 1997, PASP, 109, 1377
Shioya, Y., Bekki, K., Couch, W., & De Propris, R. 2002, ApJ, 565, 223
Smith, R. J., Lucey, J. R., Hudson, M. J., Schlegel, D. J., & Davies, R. L. 2000, MNRAS, 313, 469
Smith, R. J., et al. 2004, AJ, 128, 1558
Stanford, S. A., Eisenhardt, P. R., & Dickinson, M. 1995, ApJ, 450, 512
———. 1998, ApJ, 492, 461
Strazzullo, V., et al. 2006, A&A, 450, 909
Strom, K. M., & Strom, S. E. 1978, AJ, 83, 73
Tamura, N., & Ohta, K. 2003, AJ, 126, 596
Terlevich, A. I., Caldwell, N., & Bower, R. G. 2001, MNRAS, 326, 1547
Thuan, T. X., & Gunn, J. E. 1976, PASP, 88, 543
Trager, S. C., Faber, S. M., Worthey, G., & Gonzalez, J. J. 2000, AJ, 120, 165
Valdes, F. 1982, Proc. SPIE, 331, 465
van Dokkum, P. G., Franx, M., Fabricant, D., Illingworth, G. D., & Kelson, D. D. 2000, ApJ, 541, 95
van Dokkum, P. G., Stanford, S. A., Holden, B. P., Eisenhardt, P. R., Dickinson, M., & Elston, R. 2001, ApJ, 552, L101
Vazdekis, A., Kuntschner, H., Davies, R. L., Arimoto, N., Nakamura, O., & Peletier, R. 2001, ApJ, 551, L127
Wake, D. A., Collins, C. A., Nichol, R. C., Jones, L. R., & Burke, D. J. 2005, ApJ, 627, 186